J. Mater. Environ. Sci. 6 (10) (2015) 3066-3085
ISSN: 2028-2508
CODEN: JMESCN

PROOOOOOOOOOOOOOF

4-Aminoantipyrine Schiff base derivatives as novel corrosion inhibitors for Q235 steel in hydrochloric acid medium

A.M. Eldesoky [1], M.M. Ghoneim [2], M.A. Diab [3,+], A.A. El-Bindary [3], A.Z. El-Sonbati [3], M.K. Abd El-Kader [3,*]

[1] *Engineering Chemistry Department, High Institute of Engineering & Technology (New Damietta), Egypt and Al-Qunfudah Center for Scientific Research (QCSR), Al-Qunfudah University College, Umm Al-Qura University, KSA*
[2]*Chemistry Department, Faculty of Science, Tanta University, Tanta, Egypt*
[3]*Chemistry Department, Faculty of Science, Damietta University, Damietta 34517, Egypt*

Received 25 May 2015, Revised 30 Sep 2015, Accepted 010ct 2015
[*]*Corresponding author: E-mail: m.adiab@yahoo.com*

Abstract

The inhibitive effect of newly synthesized 4-aminoantipyrine Schiff base derivatives (1-3) against Q235 steel and its adsorption behavior were investigated in 2 M HCl solution using weight-loss method, potentiodynamic polarization, electrochemical impedance spectroscopy (EIS) and electrochemical frequency modulation (EFM) techniques. The results showed that the inhibition efficiency increased with the increase of the inhibitor concentration. The 4-aminoantipyrine Schiff base derivatives are a mixed-type inhibitor whose adsorption behavior onto Q235 steel can be well fitted by Temkin isotherm equation. The quantum chemistry was used to gain some insight, about structural and electronic effects in relation to the inhibiting efficiencies. EIS spectra exhibit one capacitive loop and confirm the inhibitive ability. X-ray diffraction patterns (XRD) for both compounds (1 and 2) show polycrystalline nature and compound (3) shows a mixture of amorphous and polycrystalline nature. Molecular docking was used to predict the binding between 4-aminoantipyrine Schiff base derivatives with the receptor of 3hb5- oxidoreductase receptor of breast cancer.

Keywords: Q235 steel, 4-Aminoantipyrine, Adsorption, Quantum chemical parameters, Molecular docking.

1. Introduction

Acid solutions are widely used in industry, such as acid pickling of iron and steel, chemical cleaning and processing, ore production and oil well acidification [1–3]. The problems arising from acid corrosion required the development of various corrosion control techniques among which the application of chemical inhibitors has been acknowledged as most economical method for preventing acid corrosion [4–9]. Many organics, such as quaternary ammonium salts, acetylenic alcohol, and heterocyclic compounds are widely used as inhibitors in various industries. The organic molecules adsorb on the metal surface through heteroatom, such as nitrogen, oxygen and sulfur, blocking the active sites and generating a physical barrier to reduce the transport of corrosive species to the metal surface [10–16]. Other researches revealed that the adsorption is influenced not only by the nature and surface charge of the metal, but also by the chemical structure of inhibitors. Among these organic compounds, heterocyclic substances containing nitrogen atoms, such as 4-aminoantipyrine compounds are considered to be excellent corrosion inhibitors in combating acidic corrosion due to high inhibition efficiency, good thermal stability and lack of irritating odor for many metals and alloys in various aggressive media [17–22]. Therefore, the develop of novel modified inhibitors containing 4-aminoantipyrine heterocyclic ring and the study of the relations between the chemical structure of inhibitors and their inhibition performances are of great importance, both from the industrial and theoretical points of view.

This paper aims to investigate the inhibition effect and electrochemical behavior of newly synthesized 4-aminoantipyrine Schiff base derivatives (1-3) for Q235 steel in 2 M HCl solution by the weight-loss method, potentiodynamic polarization, electrochemical impedance spectroscopy (EIS) and electrochemical frequency modulation (EFM) techniques. Several quantum-chemistry calculations have been performed in order to relate the inhibition efficiency to the molecular properties of the different types of compounds [23–25].

2. Experimental

2.1. Measurements

Structural analysis of the inhibitors are performed at room temperature by Philips X-ray diffractometer equipped with utilized monochromatic Cu Kα radiation (λ=1.5418Å).

The molecular structures of the investigated compounds are optimized by HF method with 3-21G basis set. The molecules are built with Perkin Elmer Chem Biodraw and optimized using Perkin Elmer Chem Bio 3D software. Accelrys (Material Studio Version 4.4) software for quantum chemical calculations has been used.

In the study simulates the actual docking process in which the ligand–protein pair-wise interaction energies are calculated using Docking Server [26]. The MMFF94 Force field was for used energy minimization of ligand molecule using Docking Server. Gasteiger partial charges were added to the ligand atoms. Non-polar hydrogen atoms were merged, and rotatable bonds were defined. Docking calculations were carried out on 3hb5–OXIDORDUCTASE–Hormone protein model. Essential hydrogen atoms, Kollman united atom type charges, and solvation parameters were added with the aid of Auto Dock tools [27]. Affinity (grid) maps of 20X20X20 A grid points and. 375 A spacing were generated using the Autogrid program [28]. Auto Dock parameter set- and distance-dependent dielectric functions were used in the calculation of the van der Waals and the electrostatic terms, respectively.

2.2. Material and medium

Q235 steel was used for the corrosion measurement. Its composition (wt %) is 0.16 C, 0.30 Si, 0.53 Mn, <0.055 S, <0.045 P, Fe balance. The aggressive solution (2 M HCl) was prepared by dilution of HCl (analytical grade, 37 %) with double distilled water. The 4-aminoantipyrine Schiff base derivatives used for this study, whose structures were shown in Table (1), were prepared in the lab as following [29]: ethanolic solutions of 4-aminoantipyrine (0.1 mol) and *P*-derivatives benzaldehyde (0.1 mol) were refluxed together for 4 h over a steam bath. The excess solvent was removed by evaporation and the concentrated solution was cooled in an ice bath with stirring. The Schiff base (L_n) which separated out as a colored powder and then recrystallized from ethanol. Our synthetic route of Schiff base ligands is shown in Scheme 1.

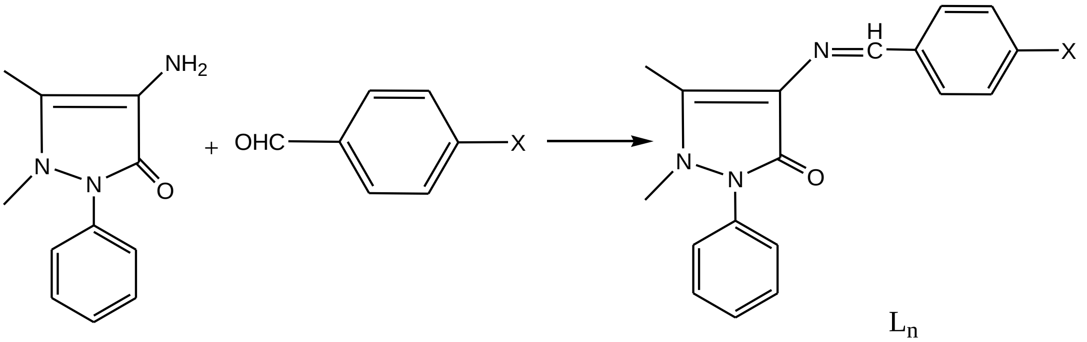

L_n

X= $-OCH_3$ (1) , -H (2), $-NO_2$ (3)

Scheme 1: Synthetic route of 4-aminoantipyrine derivatives.

2.3. Methods

2.3.1. Weight loss measurements

Rectangular specimens of Q235 steel with dimensions 2.0 x 2.0 x 0.2 cm were abraded with different grades of emery paper, degreased with acetone, rinsed with bidistilled water and dried between filter papers. After weighting accurately, the specimens were immersed in 100 ml of 2 M HCl with and without different concentrations of inhibitors at (30 ± 1°C). After different immersion periods, the Q235 steel samples were taken out, washed with bidistilled water, dried and weighted again. The weight loss values are used to calculate the corrosion rate (R) in mmy^{-1} by Eq. (1):

$$R = (\text{weight loss in gram} \times 8.75 \times 10^4) / DAT \qquad (1)$$

where D is Fe density in g cm^{-3}, A is exposed area in cm^2, T is exposure time in hr. The inhibition efficiency (%IE) and the degree of surface coverage (θ) were calculated from Eq. (2):

$$\% IE = \theta \times 100 = [(R^* - R) / R^*] \times 100 \qquad (2)$$

where R^* and R are the corrosion rates of Q235 steel in the absence and in the presence of inhibitor, respectively.

2.3.2. Electrochemical measurements

Electrochemical measurements were conducted in a conventional three electrodes thermostated cell assembly using a Gamry potentiostat/galvanostat/ZRA (model PCI300/4). A platinum foil and saturated calomel electrode (SCE) were used as counter and reference electrodes, respectively. The Q235 steel electrodes were 1x1 cm and were welded from one side to a copper wire used for electrical connection. The electrodes were abraded, degreased and rinsed as described in weight loss measurements. All experiments were carried out at temperature (30 ± 1°C). The potentiodynamic curves were recorded from -500 to 500 mV at a scan rate 1 mV S^{-1} after the steady state is reached (30 min) and the open circuit potential (OCP) was noted. The % IE and degree of surface coverage were calculated from Eq. (3):

$$IE\ \% = \theta \times 100 = [1 - (i°_{corr} / i_{corr})] \times 100 \qquad (3)$$

where i^0_{corr} and i_{corr} are the corrosion current densities of uninhibited and inhibited solution, respectively.

Table 1: Molecular structures, names, molecular weights and molecular formulas of investigated compounds.

Compound No	**Structure**	**Name**	**Mol. Wt. / Mol. Formula**
(1)	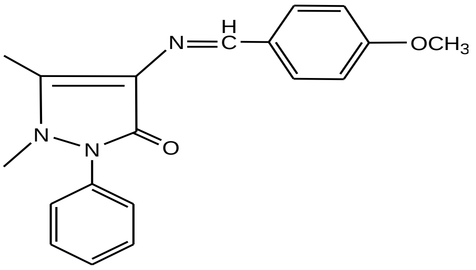	4-[(4-Methoxy-benzylidene)-amino]-1,5-dimethyl-2-phenyl-1,2-dihydro-pyrazol-3-one	321.0 / $C_{19}H_{19}N_3O_2$
(2)	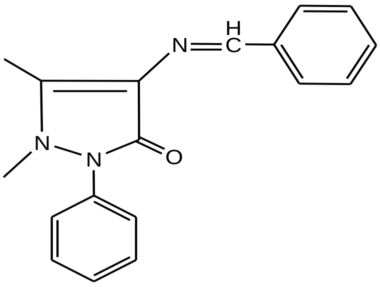	4-(Benzylidene-amino)-1,5-dimethyl-2-phenyl-1,2-dihydro-pyrazol-3-one	291.0 / $C_{18}H_{17}N_3O$
(3)	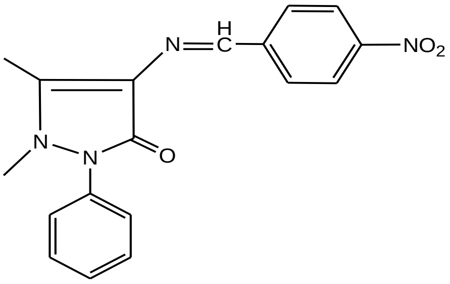	1,5-Dimethyl-4-[(4-nitro-benzylidene)-amino]-2-phenyl-1,2-dihydro-pyrazol-3-one	336.0 /$C_{18}H_{16}N_4O_3$

Electrochemical impedance spectroscopy (EIS) and electrochemical frequency modulation (EFM) experiments were carried out using the same instrument as before with a Gamry framework system based on ESA400. Gamry applications include software EIS300 for EIS measurements and EFM140 for EFM measurements; computer was used for collecting data. Echem Analyst 5.5 Software was used for plotting, graphing and fitting data. EIS measurements were carried out in a frequency range of 100 kHz to 10 mHz with amplitude of 5 mV peak-to-peak using ac signals at respective corrosion potential. EFM carried out using two frequencies 2 and 5 Hz. The base frequency was 1 Hz. In this study, we use a perturbation signal with amplitude of 10 mV for both perturbation frequencies of 2 and 5 Hz.

3. Results and discussion

3.1. Weight loss measurements

Figure (1) shows the weight loss–time curves for the corrosion of Q235 steel in 2 M HCl in the absence and presence of different concentrations of compound (1) at 30 ± 1°C .Similar curves for other compounds were obtained and are not shown. The data of Table (2) show that, the inhibition efficiency increases with increase in inhibitor concentration from 1 x 10^{-6} to 11 x 10^{-6} M. The maximum inhibition efficiency was achieved at 11 x 10^{-6} M. The lowest inhibition efficiency (%IE) is obtained in the presence of compound (3), therefore %IE tends to decrease in the following order: compound (1) > compound (2) > compound (3).

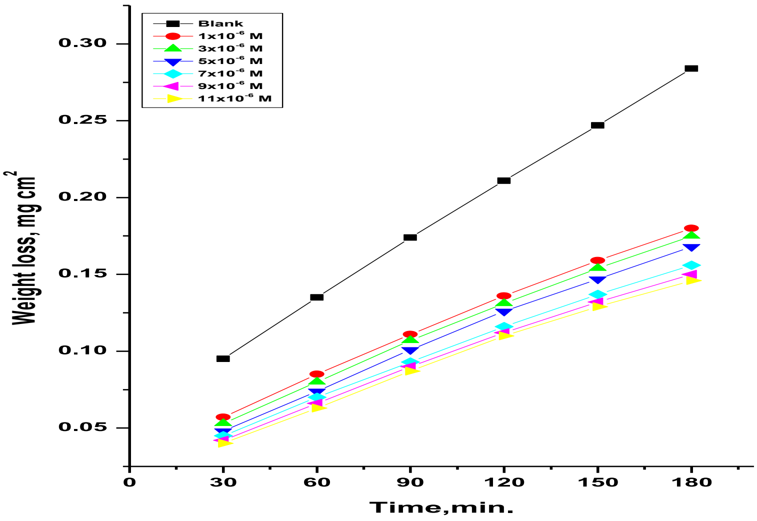

Figure 1: Weight loss-time curves for Q235 steel dissolution in 2 M HCl in the absence and presence of different concentrations of inhibitor (1) at 30 ± 1 °C.

Table 2: Variation of inhibition efficiency (% IE) of different compounds with their molar concentrations from weight loss measurements at 120 min immersion in 2 M HCl at 30 ± 1°C.

Conc. (M)	Inhibition efficiency (% IE)		
	Compound (1)	**Compound (2)**	**Compound (3)**
$1x10^{-6}$	35.5	31.8	28.4
$3x10^{-6}$	37.9	34.6	28.9
$5x10^{-6}$	40.3	36.0	30.8
$7x10^{-6}$	45.0	39.3	34.6
$9x10^{-6}$	46.9	44.1	40.3
$11x10^{-6}$	47.9	45.5	41.7

3.1.1. Adsorption isotherm

It is widely acknowledge that adsorption isotherm provide useful insight onto the mechanism of corrosion inhibition as well as the interaction among the adsorbed molecules themselves and their interaction with the electrode surface [30]. In this study, Temkin adsorption isotherm was found to be suitable for the experimental results. The isotherm is described by the following equation:

$$\theta = 2.303/a \log K_{ads} + 2.303/a \log C \qquad (4)$$

where C is the inhibitor concentration, K_{ads} is the adsorption equilibrium constant. The plot of θ versus log C was linear relation (shown in Figure 2). And the adsorption equilibrium constant K_{ads} can be calculated from the intercept. Also ΔG^o_{ads} can be calculated from the following equation:

$$\log K_{ads} = -\log 55.5 - \Delta G^o_{ads} / 2.303RT \qquad (5)$$

where value of 55.5 is the concentration of water in solution in mole/liter [31], R is the universal gas constant and T is the absolute temperature. It was appear that the value of ΔG^o_{ads} has a negative sign ensure the spontaneity of the adsorption and stability of the adsorbed layer on the alloy surface [32]. Also the values of ΔG^o_{ads} around 40 kJ mol^{-1} which was attributed to electrostatic interaction between inhibitors species and the charged metal surface ensure physisorption reaction. From Table (3), the values of K_{ads} were found to run parallel to the % IE [K (1) > K (2) > K (3)].This result reflects the increasing capability, due to structural formation, on the alloy surface [33].

Table 3: Inhibitor binding constant (K_{ads}), free energy of binding ($\Delta G_{ads.}$) and later interaction parameter (a) for inhibitors at 30 ± 0.1 °C.

Inhibitors	Temkin isotherm		
	A	K_{ads}, M^{-1}	$-\Delta G_{ads}$, $kJmol^{-1}$
Compound (1)	88.57	1.32	10.82
Compound (2)	82.25	1.25	10.68
Compound (3)	79.41	1.19	10.57

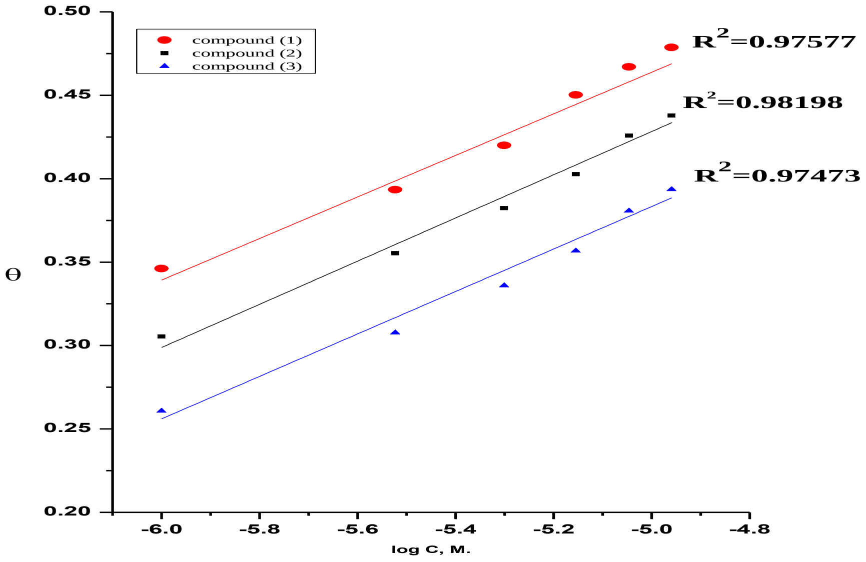

Figure 2: Curve fitting of corrosion data for Q235 steel in 2 M HCl in presence of different concentrations of inhibitors to the Temkin isotherm at 30 ± 0.1 °C.

3.1.2. Effect of temperature

The activation energies (E^*_a) for the corrosion of Q235 steel in the absence and presence of different concentrations of 4-aminoantipyrine Schiff base derivatives (1-3) were calculated using Arrhenius-type equation [34]:

$$\log k = \log A - E^*_a / 2.303RT \qquad (6)$$

where A is the pre-exponential factor, k is the rate constant, E_a^* is the apparent activation energy of the corrosion process, R is the universal gas constant and T is the absolute temperature. Arrhenius plots of log k vs. 1/T for Q235 steel in 2 M HCl in the absence and presence of different concentration of inhibitors (1) are shown graphically in Figure (3). The variation of log k *vs.* 1/T is a linear line. The values of E^*_a were calculated from the slope of these lines and given in Table (4). The increase in E^*_a by the addition of concentration of inhibitors (1-3) indicating that the energy barrier for the corrosion reaction increases. It is also indicated that the whole process is controlled by surface reaction, since the activation energy of the corrosion process is larger than 20 kJ mol^{-1} [35].Enthalpy and entropy of activation (ΔH^*, ΔS^*) for the corrosion of Q235 steel in 2 M HCl were obtained by applying the transition state equation (7) :

$$k = (RT/Nh) \exp(\Delta S^*/R) \exp(-\Delta H^*/RT) \qquad (7)$$

where *h* is Planck's constant, *N* is Avogadro's number. A plot of log k/T vs 1/T also gave straight lines as shown in Figure (4) for Q235 steel dissolution in 2 M HCl in the absence and presence of different concentration of inhibitor (1). The slopes of these lines equal $-\Delta H^*/2.303R$ and the intercept equal $\log RT/Nh + (\Delta S^*/2.303R)$ from which the value of ΔH^* and ΔS^* were calculated and tabulated in Table (4).

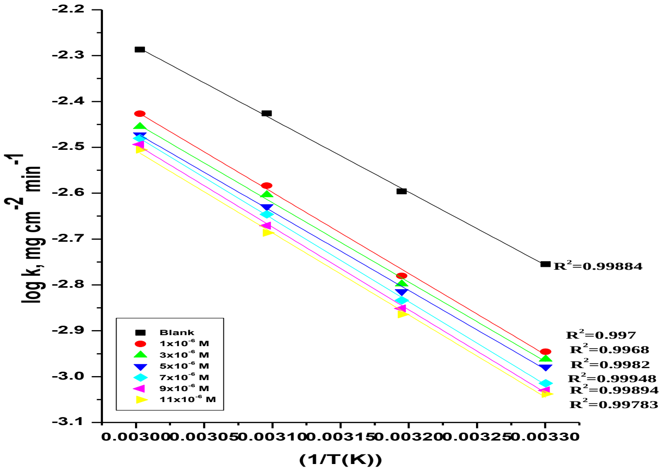

Figure 3: Arrehenius plots (log k vs 1/T) for Q235 steel in 2 M HCl in absence and presence of different concentration of inhibitor (1).

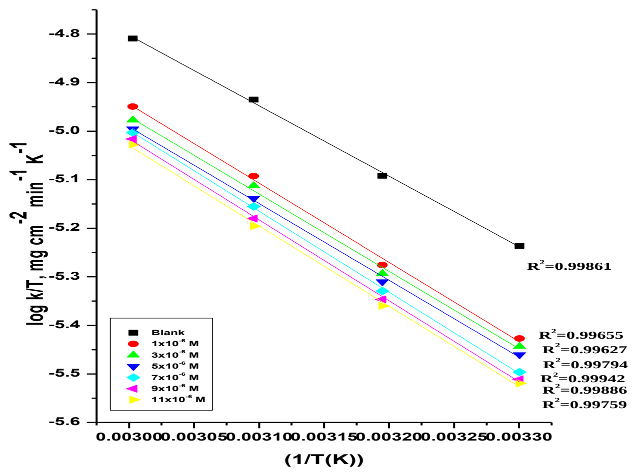

Figure 4: Transition state plots (log k/T vs 1/T) for Q235 steel in 2 M HCl in absence and presence of different concentration of inhibitor (1).

Table 4: Thermodynamic activation parameters for the dissolution of Q235 steel in 2 M HCl in the absence and presence of different concentrations of investigated compounds.

Inhibitor	Conc., M.	E_a^*, (kJ mol^{-1})	ΔH^*, (kJ mol^{-1})	$-\Delta S^*$, (J mol^{-1} K^{-1})
Blank	Blank	30.42	27.78	206.17
Compound (1)	1x10^{-6}	33.05	31.21	198.60
	3x10^{-6}	33.14	31.25	198.42
	5 x10^{-6}	33.89	31.29	197.76
	7x10^{-6}	34.18	31.54	197.43
	9x10^{-6}	34.24	31.70	197. 05
	11x10^{-6}	34.27	31.93	196.97
Compound (2)	1x10^{-6}	32.17	30.07	204.92
	3x10^{-6}	32.63	30.09	203.36
	5 x10^{-6}	32.90	30.30	202.92
	7x10^{-6}	32.92	30.48	202.095
	9x10^{-6}	34.11	31.17	199.41
	11x10^{-6}	34.14	31.75	198.13
Compound (3)	1x10^{-6}	32.05	29.24	205.81
	3x10^{-6}	32.52	29.28	204.16
	5 x10^{-6}	32.74	30.10	203.09
	7x10^{-6}	32.83	30.33	203.04
	9x10^{-6}	33.99	31.16	199.88
	11x10^{-6}	34.04	31.63	199.37

From these results, it is clear that the presence of the tested compounds increased the activation energy values and consequently decreased the corrosion rate of the Q235 steel. These results indicate that these tested compounds acted as inhibitors through increasing activation energy of Q235 steel dissolution by making a barrier to mass and charge transfer by their adsorption on Q235 steel surface. Positive sign of the enthalpies reflects the endothermic nature of the Q235 steel dissolution process.

All values of E^*_a E are larger than the analogous values of ΔH^* indicating that the corrosion process must involved a gaseous reaction, simply the hydrogen evolution reaction, associated with a decrease in the total reaction volume [36]. The values of ΔS^* in absence and presence of the tested compounds are large and negative; this indicates that the activated complex in the rate-determining step represents an association rather than dissociation step, meaning that a decrease in disordering takes place on going from reactants to the activated complex [37, 38].

3.2. Potentiodynamic polarization measurements

Polarization measurements were carried out in order to gain knowledge concerning the kinetics of the cathodic and anodic reactions. Figure (5): shows the polarization behavior of Q235 steel electrode in 2 M HCl in the absence and presence of various concentrations of compound (1). Figure (5) shows that both the anodic and cathodic reactions are affected by the addition of investigated organic derivatives and the inhibition efficiency increases as the inhibitor concentration increases, but the cathodic reaction is more inhibited, meaning that the addition of organic derivatives reduces the anodic dissolution of Q235 steel and also retards the cathodic reactions. Therefore, investigated organic derivatives are considered as mixed type inhibitors.

The values of electrochemical parameters such as corrosion current densities (i_{corr}), corrosion potential (E_{corr}), the cathodic Tafel slope (β_c), anodic Tafel slope (β_a) and inhibition efficiency (% IE) were calculated from the curves of Figure (5) and are listed in Table (5). The results in Table (5) revealed that the corrosion current density decreases obviously after the addition of inhibitors in 2 M HCl and % IE increases with increasing the inhibitor concentration. In the presence of inhibitors E_{corr} was enhanced with no definite trend, indicating that these compounds act as mixed–type inhibitors in 2 M HCl. The inhibition efficiency was calculated using equation:

$$\% \ IE_p = [\, i^o_{corr} - i_{corr}) / \, i^o_{corr}] \, x100 \qquad (8)$$

where i^o_{corr} and i_{corr} are the uninhibited and inhibited corrosion current densities, respectively.

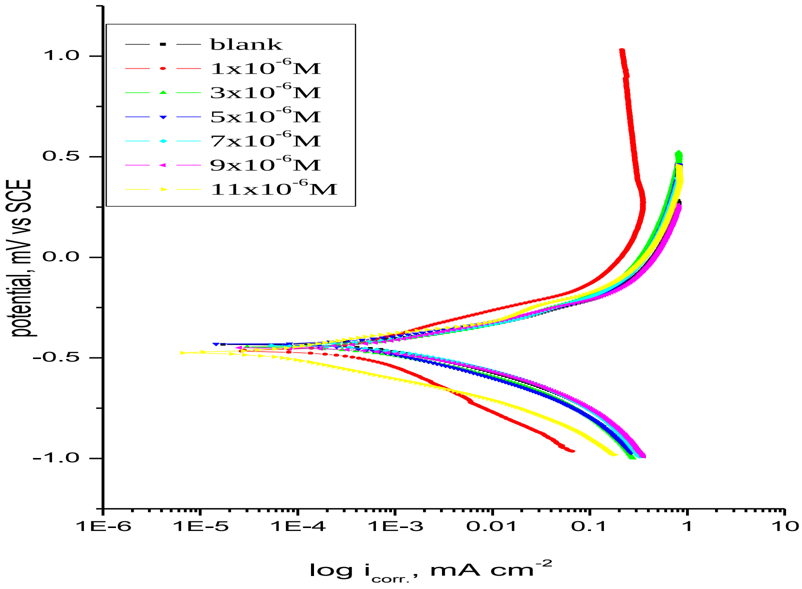

Figure 5: Potentiodynamic polarization curves for the corrosion of Q235 steel in 2 M HCl in the absence and presence of various concentrations of compound (1) at 30 ± 0.1 °C.

It is obvious from Table (5) that the slopes of the anodic (β_a) and cathodic (β_c) Tafel lines remain almost unchanged upon addition of organic derivatives, giving rise to a nearly parallel set of anodic lines, and almost parallel cathodic plots results too. Thus the adsorbed inhibitors act by simple blocking of the active sites for both anodic and cathodic processes. In other words, the adsorbed inhibitors decrease the surface area for corrosion without affecting the corrosion mechanism of Q235 steel in 2 M HCl solution, and only causes inactivation of a part of the surface with respect to the corrosive medium [39,40].

Table 5: Effect of concentrations of the investigated compounds (1-3) on the free corrosion potential ($E_{corr.}$), corrosion current density ($i_{corr.}$), Tafel slopes (β_a& β_c), ,degree of surface coverage (θ) and inhibition efficiency (% IE) for Q235 steel in 2 M HCl at 30 ± 0.1 °C.

Conc., M		$i_{cor\ X\ 10^{-4}}$, mA cm^{-2}	$-E_{corr}$ mV vs(SCE)	β_a X 10^{-3}, mV dec^{-1}	β_c X 10^{-3}, mV dec^{-1}	Θ	% IE
2 M HCl		7.90	434	107.7	146.9	-	-
Compound (1)	1 x 10^{-6}	4.57	464	196.1	187.8	0.4215	42.15
	3 x 10^{-6}	4.43	446	81.1	105.5	0.4392	43.92
	5 x 10^{-6}	3.89	431	77.6	121.9	0.5075	50.75
	7 x 10^{-6}	1.60	438	42.2	41.6	0.7974	79.74
	9 x 10^{-6}	1.44	449	43.6	35.9	0.8177	81.77
	11x 10^{-6}	1.04	473	125.9	239.7	0.8683	86.83
Compound (2)	1 x 10^{-6}	6.04	448	11.5	86.2	0.2354	23.54
	3 x 10^{-6}	5.57	440	81.0	92.9	0.2949	29.49
	5 x 10^{-6}	5.40	452	32.8	22.3	0.3164	31.64
	7 x 10^{-6}	5.20	452	95.4	69.9	0.3417	34.17
	9 x 10^{-6}	4.86	441	103.8	85.0	0.3848	38.48
	11x 10^{-6}	4.87	465	33.7	27.2	0.3987	39.87
Compound (3)	1 x 10^{-6}	7.77	487	118.3	120.1	0.164	1.64
	3 x 10^{-6}	7.70	467	112.8	132.3	0.253	2.53
	5 x 10^{-6}	7.62	450	125.4	84.2	0.356	3.56
	7 x 10^{-6}	7.37	483	85.9	122.0	0.670	6.70
	9 x 10^{-6}	6.62	457	114.8	95.7	0.1620	16.20
	11x 10^{-6}	6.39	447	35.0	31.6	0.1911	19.11

The inhibition efficiency of these compounds follows the sequence: compound (1) > compound (2) > compound (3). This sequence may attribute to free electron pair in nitrogen atom, π electrons on aromatic nuclei and the substituent in the molecular structure of the inhibitor, and again reflects, as confirmed from weight loss measurements, the increased ability of compound (1) to inhibit 2 M HCl acid corrosion of Q235 steel as compared to compound (3). This is clearly seen from the highest efficiency recorded for compound (3).

3.3. Electrochemical impedance spectroscopy (EIS)

EIS is well-established and powerful technique in the study of corrosion. Surface properties, electrode kinetics and mechanistic information can be obtained from impedance diagrams [41-45]. Figure (6) shows Nyquist (a) and Bode (b) plots obtained at open-circuit potential both in the absence and presence of increasing concentrations of investigated compounds at 30 ± 0.1 °C. The increase in the size of the capacitive loop with the addition of organic derivatives shows that a barrier gradually forms on the copper surface. The increase in the capacitive loop size Figure 6(a) enhances, at a fixed inhibitor concentration, following the order: compound (1) > compound (2) > compound (3), confirming the highest inhibitive influence of compound (1).

The Nyquist plots do not yield perfect semicircles as expected from the theory of EIS. The deviation from ideal semicircle was generally attributed to the frequency dispersion [46] as well as to the inhomogenities of the surface. EIS spectra of the organic additives were analyzed using the equivalent circuit, Figure (7), which represents a single charge transfer reaction and fits well with our experimental results. The constant phase element, CPE, is introduced in the circuit instead of a pure double layer capacitor to give a more accurate fit [47]. The double layer capacitance, C_{dl}, is calculated from Eq. (9):

$$C_{dl} = Y_0\ \omega^{n-1} / \sin\ [n\ (\pi/2)] \qquad (9)$$

where Y_0 is the magnitude of the CPE, $\omega = 2\pi f_{max}$, f_{max} is the frequency at which the imaginary component of the impedance is maximal and the factor n is an adjustable parameter that usually lies between 0.50 and 1.0.

After analyzing the shape of the Nyquist plots, it is concluded that the curves approximated by a single capacitive semicircles, showing that the corrosion process was mainly charged-transfer controlled [48-50]. The general shape of the curves is very similar for all samples (in presence or absence of inhibitors at different immersion times) indicating that no change in the corrosion mechanism [51]. From the impedance data (Table 6), we conclude that the value of R_{ct} increases with increasing the concentration of the inhibitors and this indicates an increase in % IE, which in concord with the weight loss results obtained. In fact the presence of inhibitors enhances the value of R_{ct} in acidic solution. Values of double layer capacitance are also brought down to the maximum extent in the presence of inhibitor and the decrease in the values of CPE follows the order similar to that obtained for i_{corr} in this study. The decrease in CPE/C_{dl} results from a decrease in local dielectric constant and/or an increase in the thickness of the double layer, suggesting that organic derivatives inhibit the Q235 steel corrosion by adsorption at metal/acid [52, 53]. The inhibition efficiency was calculated from the charge transfer resistance data from equation(10) [54]:

$$\% IE_{EIS} = [1 - (R^{\circ}_{ct} / R_{ct})] \times 100 \qquad (10)$$

where R^{o}_{ct} and R_{ct} are the charge-transfer resistance values without and with inhibitor, respectively.

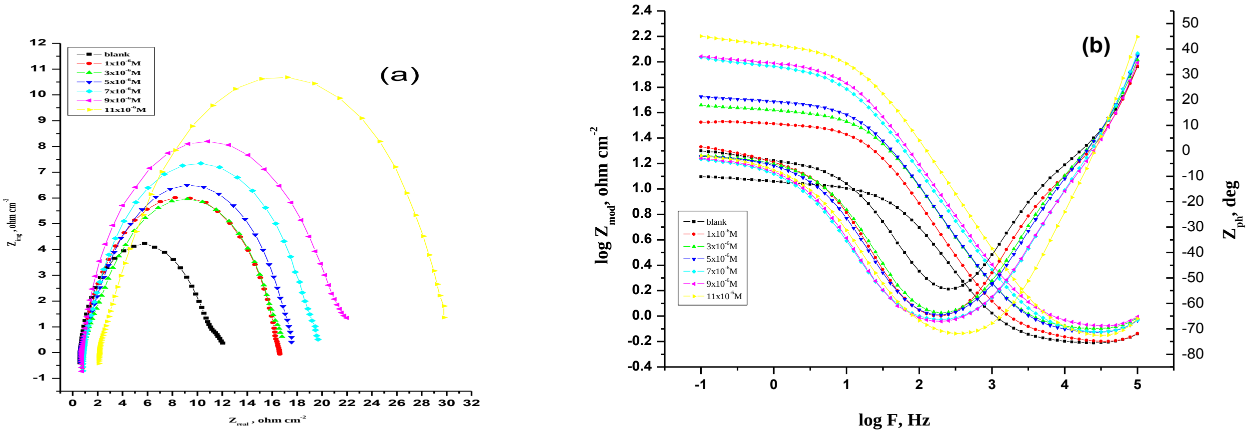

Figure 6: EIS Nyquist plots (a) and Bode plots (b) for Q235 steel surface in 2 M HCl in the absence and presence of different concentrations of compound (1) at 30 ± 0.1 °C.

Table 6: Electrochemical kinetic parameters obtained by EIS technique for Q235 steel in 2 M HCl without and with various concentrations of compounds (1-3) at 30 ± 0.1 °C.

Inhibitors	Conc., M .	R_S X 10^{-1}, Ωcm^2	Y_o, x 10^{-4} $\mu\Omega^{-1}s^n$	n X 10^{-1}	R_{ct}, Ω cm^2	C_{dl} X 10-4, μFcm^{-2}	θ	%IE
Compound (1)	Blank	6.13	6.38	8.79	10.81	9.67	------	-----
	1 x 10^{-6}	6.45	4.02	8.93	32.23	2.16	0.6645	66.45
	3 x 10^{-6}	7.92	3.19	8.80	41.47	2.04	0.7393	73.93
	5 x 10^{-6}	7.39	3.27	8.75	48.99	2.01	0.7793	77.93
	7 x 10^{-6}	7.32	2.87	8.56	95.94	1.94	0.8873	88.73
	9 x 10^{-6}	8.25	2.44	8.63	101.00	1.49	0.8929	89.29
	11x 10^{-6}	6.87	1.28	8.97	136.70	1.30	0.9209	92.09
Compound (2)	1 x 10^{-6}	8.17	3.14	8.63	15.56	5.91	0.3052	30.52
	3 x 10^{-6}	7.97	1.78	7.62	16.34	4.99	0.3384	33.84
	5 x 10^{-6}	6.53	1.66	7.80	17.38	4.78	0.3780	37.80
	7 x 10^{-6}	8.24	9.73	8.30	18.89	2.82	0.4277	42.77
	9 x 10^{-6}	7.44	7.30	8.76	20.83	2.78	0.4810	48.10
	11x 10^{-6}	6.10	2.03	7.60	29.25	2.29	0.6304	63.04
Compound (3)	1 x 10^{-6}	9.19	2.69	8.69	12.02	9.15	0.1006	10.06
	3 x 10^{-6}	7.45	1.33	8.10	12.31	9.02	0.1218	12.18
	5 x 10^{-6}	6.78	3.78	8.87	13.42	8.86	0.1944	19.44
	7 x 10^{-6}	7.35	3.19	8.73	13.78	8.72	0.2155	21.55
	9 x 10^{-6}	6.23	1.44	8.12	14.11	8.23	0.2338	23.38
	11x 10^{-6}	6.10	1.54	8.27	14.46	7.74	0.2524	25.24

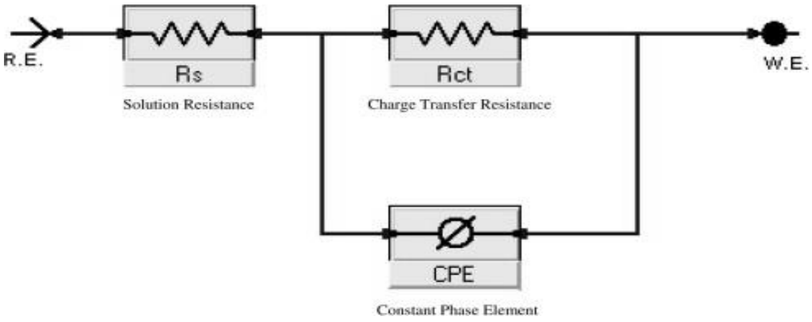

Figure 7: Equivalent circuit model used to fit experimental EIS.

3.4. Electrochemical Frequency Modulation Technique (EFM)

EFM is a nondestructive corrosion measurement technique that can directly and quickly determine the corrosion current values without prior knowledge of Tafel slopes, and with only a small polarizing signal. These advantages of EFM technique make it an ideal candidate for online corrosion monitoring [55]. The great strength of the EFM is the causality factors which serve as an internal check on the validity of EFM measurement. The causality factors CF-2 and CF-3 are calculated from the frequency spectrum of the current responses.

Figure (8) shows the EFM Intermodulation spectrums of Q235 steel in 2 M HCl solution containing different concentrations of compound (1). Similar curves were obtained for other compounds (not shown). The harmonic and intermodulation peaks are clearly visible and are much larger than the background noise. The two large peaks, with amplitude of about 200 µA, are the response to the 40 and 100 mHz (2 and 5 Hz) excitation frequencies. It is important to note that between the peaks there is nearly no current response (<100 nA). The experimental EFM data were treated using two different models: complete diffusion control of the cathodic reaction and the "activation" model. For the latter, a set of three non-linear equations had been solved, assuming that the corrosion potential does not change due to the polarization of the working electrode [56]. The larger peaks were used to calculate the corrosion current density (i_{corr}), the Tafel slopes (β_c and β_a) and the causality factors (CF-2 and CF-3).These electrochemical parameters were listed in Table (7).

The data presented in Table (7) obviously show that, the addition of any one of tested compounds at a given concentration to the acidic solution decreases the corrosion current density, indicating that these compounds inhibit the corrosion of Q235 steel in 2 M HCl through adsorption. The causality factors obtained under different experimental conditions are approximately equal to the theoretical values (2 and 3) indicating that the measured data are verified and of good quality. The inhibition efficiencies % IE_{EFM} increase by increasing the inhibitor concentrations and was calculated as from equation (11):

$$\% IE_{EFM} = [1-(i_{corr} / i^{o}_{corr})] x\ 100 \qquad (11)$$

where i^{o}_{corr} and i_{corr} are corrosion current densities in the absence and presence of inhibitor, respectively.

The inhibition sufficiency obtained from this method is in the order: compound (1) > compound (2) > compound (3).

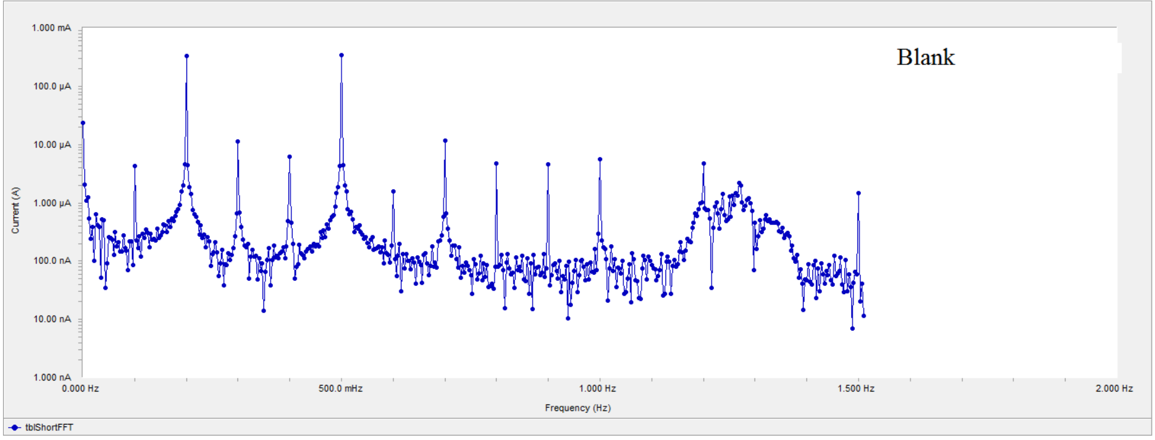

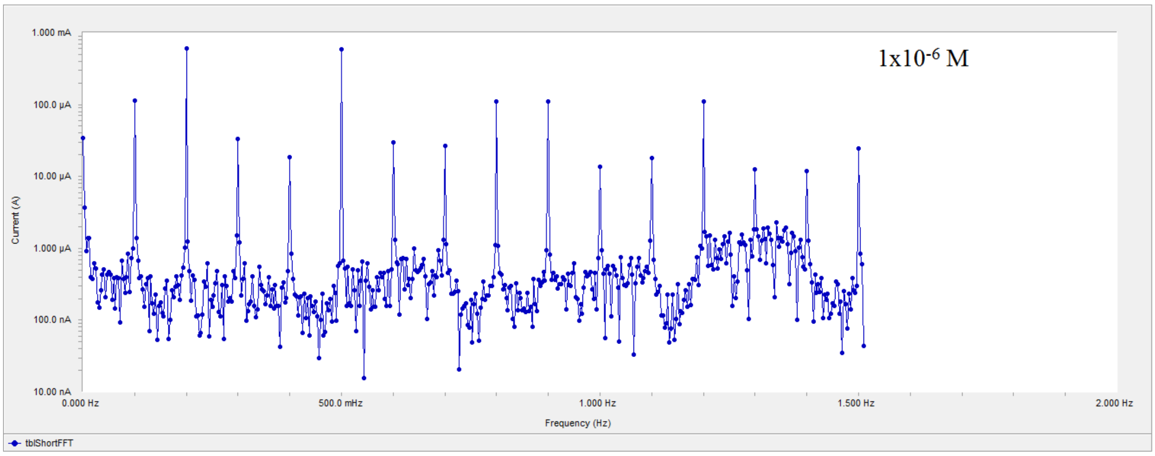
1x10-6 M
1.000 mA
100.0 µA
10.00 µA
1.000 µA
100.0 nA
10.00 nA
Current (A)
0.000 Hz
500.0 mHz
1.000 Hz
1.500 Hz
2.000 Hz
Frequency (Hz)
tblShortFFT

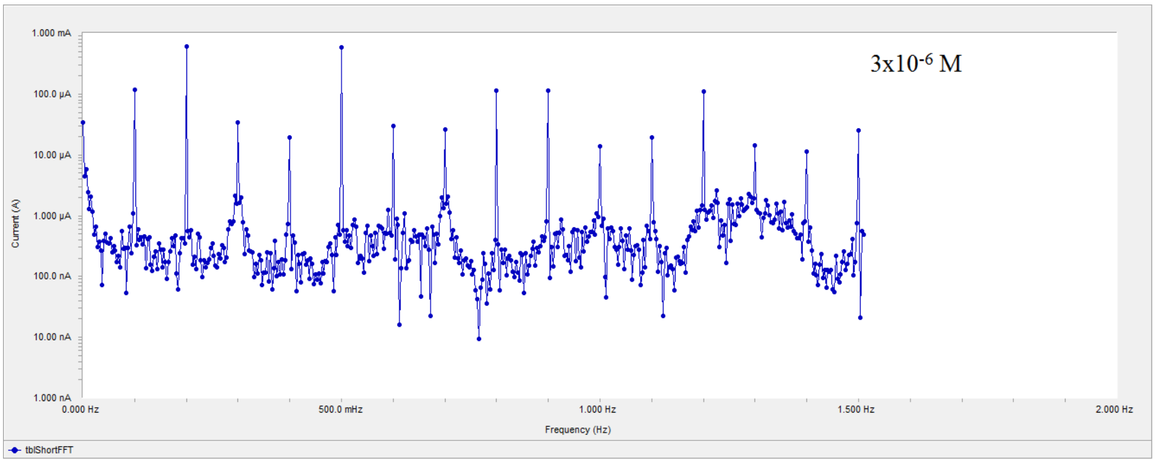
3x10-6 M
1.000 mA
100.0 µA
10.00 µA
1.000 µA
100.0 nA
10.00 nA
1.000 nA
Current (A)
0.000 Hz
500.0 mHz
1.000 Hz
1.500 Hz
2.000 Hz
Frequency (Hz)
tblShortFFT

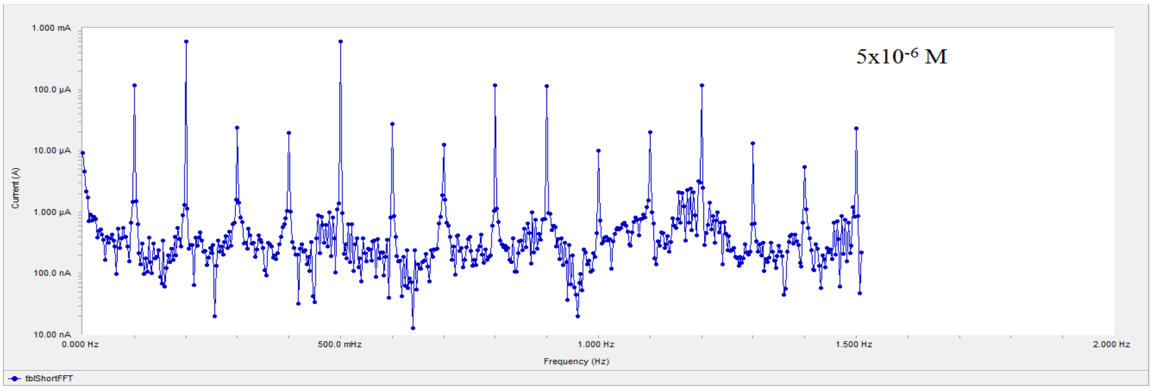
5x10-6 M
1.000 mA
100.0 µA
10.00 µA
1.000 µA
100.0 nA
10.00 nA
Current (A)
0.000 Hz
500.0 mHz
1.000 Hz
1.500 Hz
2.000 Hz
Frequency (Hz)
tblShortFFT

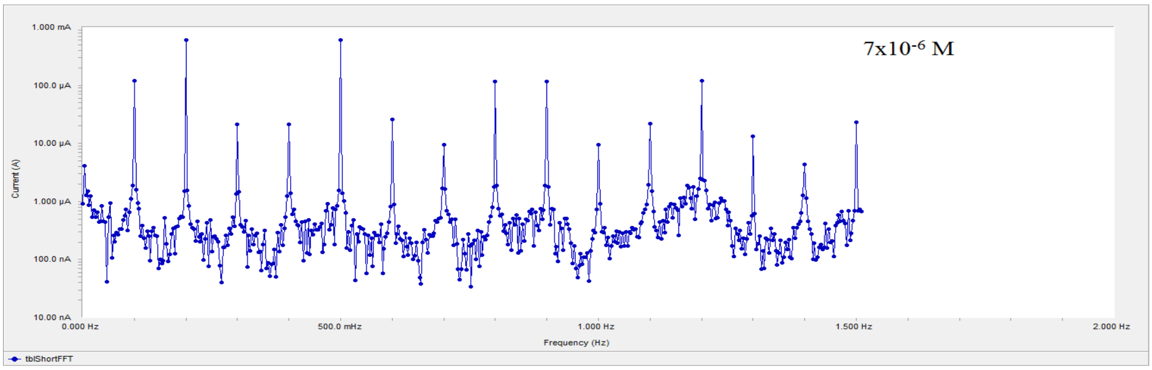
7x10-6 M
1.000 mA
100.0 µA
10.00 µA
1.000 µA
100.0 nA
10.00 nA
Current (A)
0.000 Hz
500.0 mHz
1.000 Hz
1.500 Hz
2.000 Hz
Frequency (Hz)
tblShortFFT

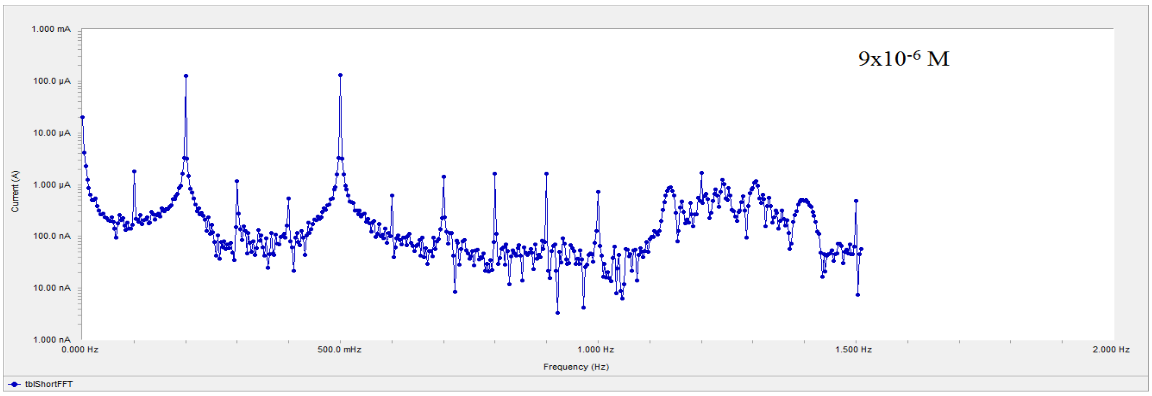

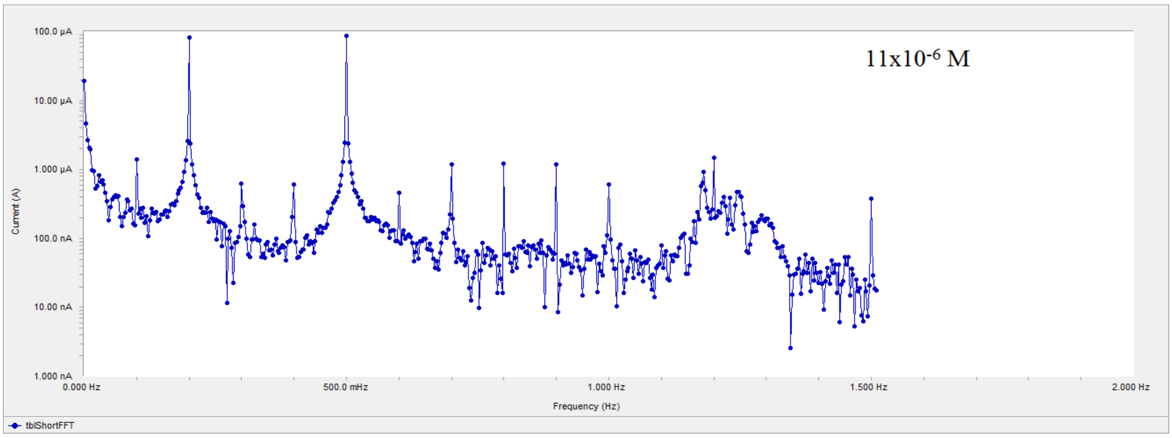

Figure 8: EFM spectra for Q235 steel in 2 M HCl in the abscence and presence of different concentration of compound (1) at 30 ± 0.1 °C.

Table 7: Electrochemical kinetic parameters obtained by EFM technique for Q235 steel in 2 M HCl without and with various concentrations of compounds (1-3) at 30 ± 0.1 °C.

Inhibitors	Conc., M .	$i_{corr.}$, $\mu A\ cm^{2}$	β_a x 10^{-3}, mV dec^{-1}	β_c x 10^{-3}, mV dec^{-1}	CF-2	CF-3	Θ	% IE
Compound (1)	Blank	520.4	907	112	1.9	3.0	-	-
	1 x 10^{-6}	243.3	255	277	2.1	3.3	0.532	53.2
	3 x 10^{-6}	242.9	256	276	1.5	3.3	0.533	53.3
	5 x 10^{-6}	240.7	255	268	1.8	2.9	0.537	53.7
	7 x 10^{-6}	239.3	254	265	1.9	2.2.7	0.540	54.0
	9 x 10^{-6}	199.2	979	104	1.8	3.1	0.617	61.7
	11x 10^{-6}	119.9	895	951	1.8	3.2	0.769	76.9
Compound (2)	1 x 10^{-6}	257.4	270	315	1.7	3.1	0.505	50.5
	3 x 10^{-6}	257.0	281	297	1.9	2.8	0.506	50.6
	5 x 10^{-6}	256.4	281	295	1.7	2. 8	0.507	50.7
	7 x 10^{-6}	252.0	274	288	1.7	3.0	0.515	51.5
	9 x 10^{-6}	247.3	266	280	2.3	2.8	0.524	52.4
	11x 10^{-6}	243.7	260	273	1.9	2.9	0.531	53.1
Compound (3)	1 x 10^{-6}	491.2	750	832	2.0	2.5	0.561	5.61
	3 x 10^{-6}	348.0	458	554	1. 9	3.7	0.331	33.1
	5 x 10^{-6}	313.9	368	423	1.7	3.0	0.396	39.6
	7 x 10^{-6}	289.3	338	350	1.8	2.9	0.444	44.4
	9 x 10^{-6}	284.1	326	345	1.9	3.0	0.454	45.4
	11x 10^{-6}	259.0	284	301	2.0	3.0	0.502	50.2

3.5. Chemical structure of the inhibitors and corrosion inhibition

Inhibition of the corrosion of Q235 steel in 2 M HCl solution by some 4-aminoantipyrine compounds is determined by weight loss, potentiodynamic anodic polarization measurements, Electrochemical Impedance Spectroscopy (EIS) and electrochemical frequency modulation method (EFM) Studies, it was found that the inhibition efficiency depends on concentration, nature of metal, the mode of adsorption of the inhibitors and surface conditions.

The observed corrosion data in presence of these inhibitors, namely:

- **i)** The decrease of corrosion rate and corrosion current with increase in concentration of the inhibitor.
- **ii)** The linear variation of weight loss with time.
- **iii)** The shift in Tafel lines to higher potential regions.
- **iv)** The decrease in corrosion inhibition efficiency with increasing temperature indicates that desorption of the adsorbed inhibitor molecules takes place.
- **v)** The inhibition efficiency depends on the number of adsorption active centers in the molecule and their charge density.

It was concluded that the mode of adsorption depends on the affinity of the metal towards the π-electron clouds of the ring system. Metals such as Fe, which have a greater affinity towards aromatic moieties, were found to adsorb benzene rings in a flat orientation. The order of decreasing the percentage inhibition efficiency of the investigated inhibitors in the corrosive solution was as follow:

compound (1) > compound (2) > compound (3).

Compound (1) exhibits excellent inhibition power due to: (i) the presence of p-OCH_3 group which is an electron donating group with negative Hammett constant (σ = -0.27), Also this group will increase the electron charge density on the molecule, and (ii) its larger molecular size that may facilitate better surface coverage.

Compound (2) comes after compound (1) in inhibition efficiency. This is due to it has lesser molecular size and has no substituent in p-position (H-atom with σ =0.0) which contributes no charge density to the molecule.

Compound (3) comes after compound (2) in inhibition efficiency due to the presence of p- NO_2 which has positive Hammett constant (σ = +0.78).i.e. group which lower the electron density on the molecule and hence, lower inhibition efficiency.

3.6. X-ray diffraction analysis

The X-ray diffraction (XRD) patterns of the inhibitors Schiff base powder are shown in Figure (9). The XRD patterns show that compound (1and 2) Schiff bases are a polycrystalline. The XRD pattern of the powder compound (3) show many peaks in addition to a broad hump at $2\Theta = 8^{o}$. This behavior indicates that the powder is a mixture of amorphous and polycrystals.

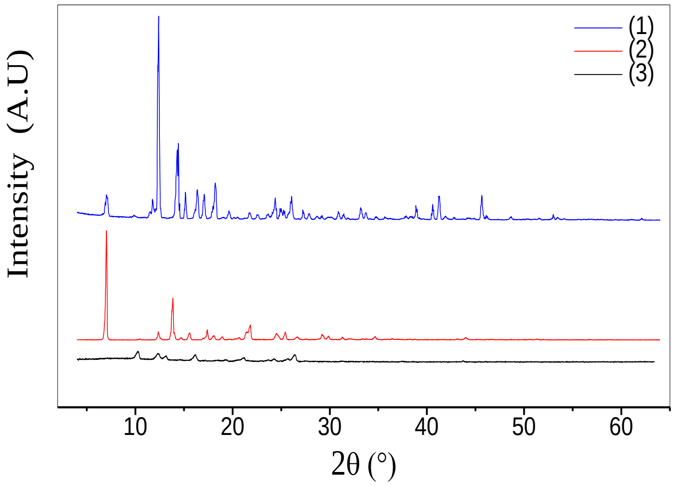

Figure 9: X-ray diffraction patterns for compound (1-3) in powder forms.

3.7. Quantum chemical calculations

Figure (10) represents the molecular orbital plots and Mulliken charges of investigated compounds. Theoretical calculations were performed for only the neutral forms, in order to give further insight into the experimental results. Values of quantum chemical indices such as energies of lowest unoccupied molecular orbitals (LUMO) and energy of highest occupied molecular orbitals (HOMO) (E_{HOMO} and E_{LUMO}), the formation heat (ΔH_f) and energy gap (ΔE) are calculated and given in Table (8). It has been reported that the higher or less negative E_{HOMO} is associated of inhibitor, the greater the trend of offering electrons to unoccupied d orbital of the metal, and the higher the corrosion inhibition efficiency, in addition, the lower E_{LUMO}, the easier the acceptance of electrons from metal surface [57]. From Table (8), it is clear that ΔE obtained by the four methods in case of compound (3) is lower than compound (1), which enhance the assumption that compound (1) molecule will absorb more strongly on Q235 steel surface than compound (3), due to facilitating of electron transfer between molecular orbital HOMO and LUMO which takes place during its adsorption on the Q235 steel surface and thereafter presents the maximum of inhibition efficiency.

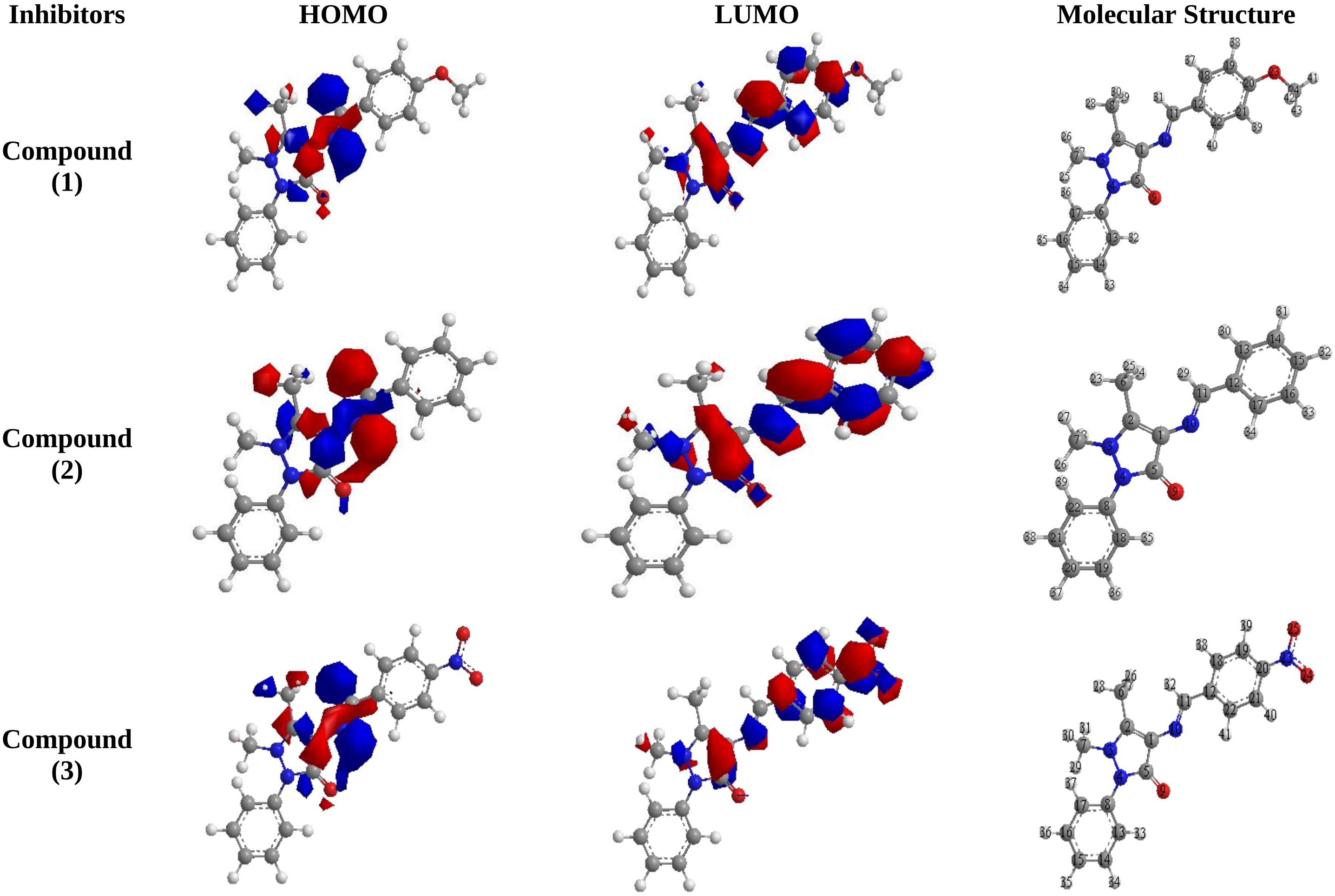

Figure 10: Molecular orbital plots of investigated compounds.

Table 8: The calculated quantum chemical properties for investigated compounds.

	Compound (1)	Compound (2)	Compound (3)
$-E_{HOMO}$ (a.u)	0.2648	0.2655	0.2684
$-E_{LUMO}$ (a.u)	0.1881	0.0701	0.0521
ΔE (a.u)	0.0770	0.1950	0.2160
η (a.u)	0.1063	0.0976	0.0401
σ (a.u)$^{-1}$	9.4073	10.2459	24.9376
-Pi (a.u)	0.1584	0.1678	0.2282
χ (a.u)	0.1584	0.1678	0.2282
S (a.u)$^{-1}$	4.7036	5.1229	12.4688
ω (a.u)	0.1180	0.1442	0.6493
ΔN_{max}	1.4901	1.7192	5.6907

Also it can be seen that E_{HOMO} increases from compound (1) to compound (3) facilitates the adsorption and the inhibition by supporting the transport process through the adsorbed layer. Reportedly, excellent corrosion inhibitors are usually those organic compounds who are not only offer electrons to unoccupied orbital of the metal, but also accept free electrons from the metal [58, 59]. It can be seen that all calculated quantum chemical parameters validate these experimental results.

3.8. Molecular docking

Cancer can be described as the uncontrolled growth of abnormal cells. Breast cancer is one of the most recurring worldwide diagnosed and deadliest cancers next to lung cancer with a high number of mortality rates among females [60]. At global level, it accounted for more than 1.6 million new cases in 2010. The incidence or prevalence rate of the breast cancer in India is expected to be more than 90,000 in the coming years and over 50,000 women die each year.

Molecular docking is a key tool in computer drug design [61]. The focus of molecular docking is to simulate the molecular recognition process. Molecular docking aims to achieve an optimized conformation for both the protein and drug with relative orientation between them such that the free energy of the overall system is minimized. In this context, we used molecular docking between compounds (1-3) and breast cancer (3hb5). The results showed a possible arrangement between compounds (1-3) and receptor 3hb5. The docking study showed a favorable interaction between compounds (1-3) and the receptor 3hb5 Figure (11,12 and 13) and the calculated energy is listed in Table 9. According to the results obtained in this study, HB plot curve indicate that the compounds (1-3) bind to the protein with hydrogen bond interactions and decomposed interaction energies in Kcal/mole were exist between compounds (1-3) with 3hb5 receptor as shown in Figure 14 and Table 10. The calculated efficiency is favorable where K_i values estimated by AutoDock were compared with experimental K_i values, when available, and the Gibbs free energy is negative. Also, based on this data, we can propose that interaction between the 3hp5 receptor and the compounds (1-3) is possible. 2D plot curves of docking with compounds (1-3) are shown in Figure 15 (a, b and c). This interaction could activate apoptosis in cancer cells energy of interactions with compounds (1-3). Binding energies are most widely used as mode of measuring binding affinity of compounds. Thus, decrease in binding energy due to mutation will increase the binding affinity of the compounds towards the receptor. The characteristic features of compounds were represented in presence of active sites available for hydrogen bonding. This feature gives them the ability to be good binding inhibitors to the protein and will help to produce augmented inhibitory compounds. As shown in Table 9, the values of K_i is related to the nature of the p-substituent as they increase according to the following order *p*-(NO_2 > H > OCH_3). This can be attributed to the fact that the effective charge increased due to the electron withdrawing p-substituent compound (3) while it decreased by the electrons donating character of compound (1). This is in accordance with that expected from Hammett's constant (σ^R) as shown in Figure 16, correlate the K_i values with σ^R it is clear that all these values increase with increasing σ^R. The results confirmed also that, the compounds derived from 4-aminoantipyrine Schiff base derivatives (1-3) are efficient inhibitors of 3hb5 – OXID ORDUCTASE breast cancer.

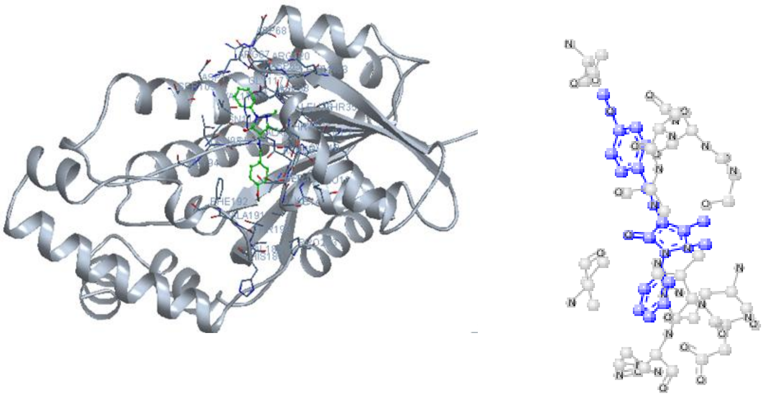
(a) (b)

Figure 11: The ligand (1) (green in (a) and blue in (b)) in interaction with receptor breast cancer mutant 3hb5. (For interpretation of the references to color in this figure legend, the reader is referred to the web version of this article).

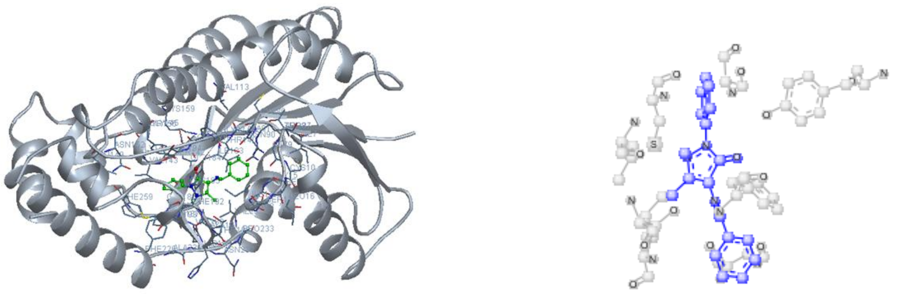

(a) (b)

Figure 12: The ligand (2) (green in (a) and blue in (b)) in interaction with receptor breast cancer mutant 3hb5. (For interpretation of the references to color in this figure legend, the reader is referred to the web version of this article).

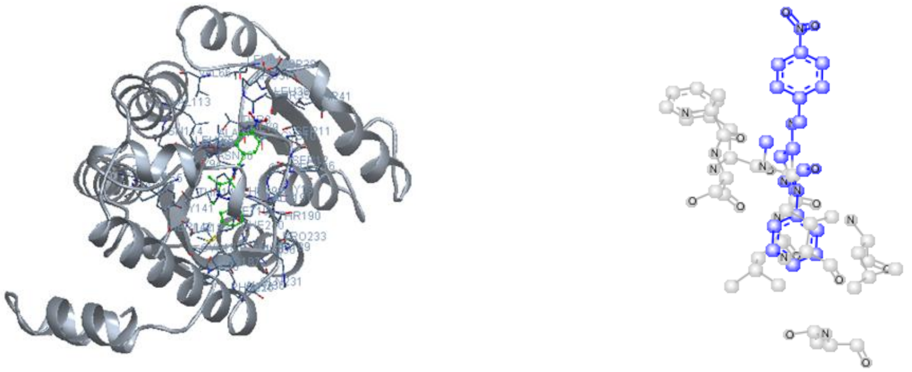

(a) (b)

Figure 13: The ligand (3) (green in (a) and blue in (b)) in interaction with receptor breast cancer mutant 3hb5. (For interpretation of the references to color in this figure legend, the reader is referred to the web version of this article).

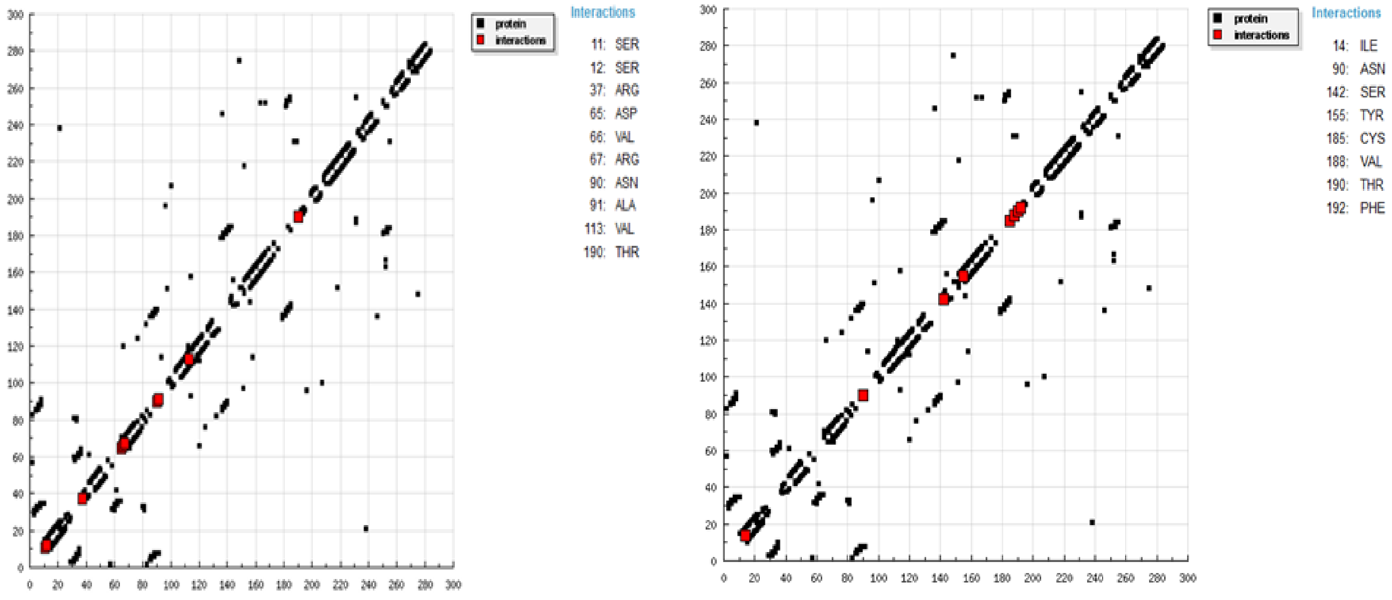

(a) (b)

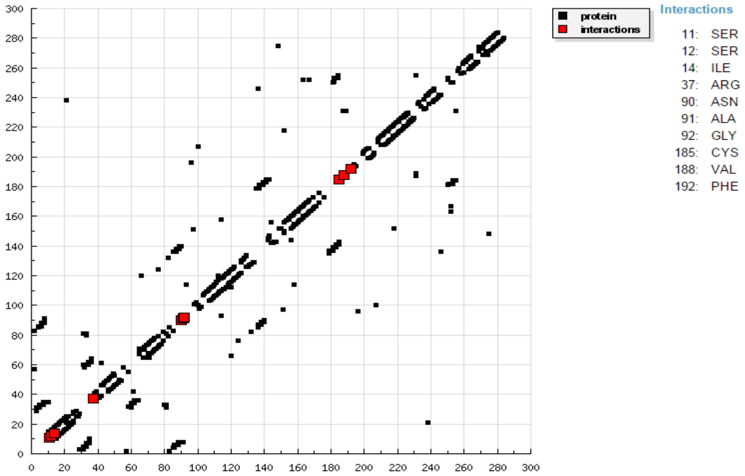

(c)

Figure 14: HB plot of interaction between ligands (a) compound (1), (b) compound (2) and (c) compound (3) with receptor breast cancer mutant 3hb5.

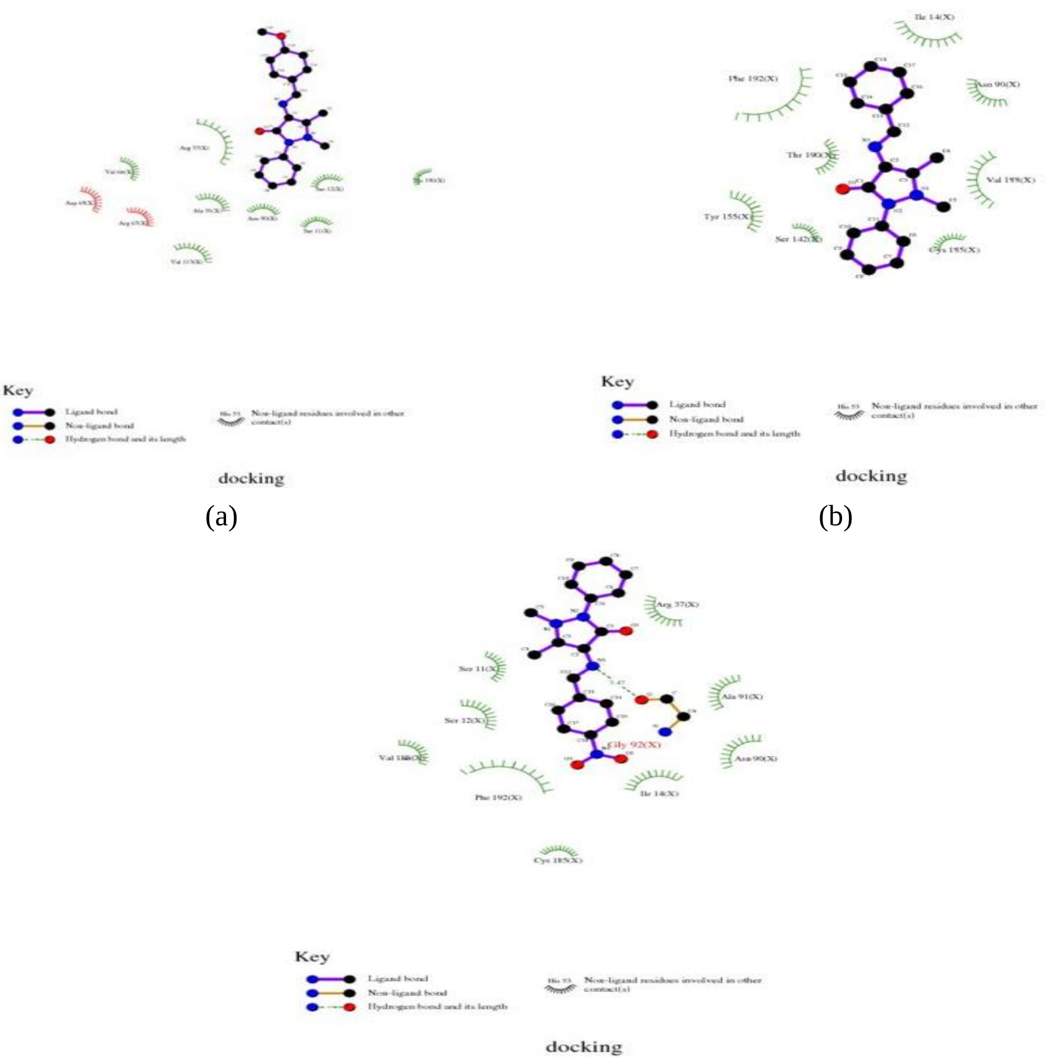

(a) (b)

(c)

Figure 15: 2D plot of interaction between ligands (a) compound (1), (b) compound (2) and (c) compound (3) with receptor breast cancer mutant 3hb5.

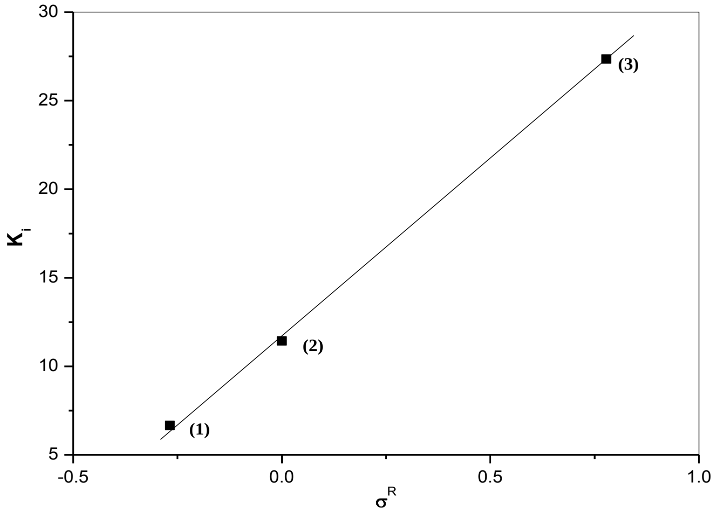

Figure 16: The relation between Hammett's substitution coefficient (σ^R) *vs.* K_i of compounds (1-3).

Table 9: Energy values obtained in docking calculations of ligands with receptor breast cancer mutant 3hb5.

Receptor	compound	Est. free energy of binding (kCal/mol)	Est. inhibition constant (K_i) (uM)	vdW+ bond+ desolv energy (kCal/mol)	Electrostatic Energy (kCal/mol)	Total intercooled Energy (kCal/mol)	Interact surface
3hb5	(1)	-7.06	6.65	-8.29	-0.05	-8.34	842.984
	(2)	-6.74	11.43	-7.73	0.01	-7.74	801.358
	(3)	-6.23	27.34	-7.44	0.04	-7.40	913.01

Table 10: Decomposed interaction energies of ligands with receptor breast cancer mutant 3hb5.

Receptor		Hydrogen bonds	Polar	Hydrophobic	Other
3hb5	(1)		ARG37 (-2.6094) THR190 (-0.3299)	VAL113 (-1.1999) ALA91 (-0.885) VAL66 (-0.6347)	ASN90 (-0.6217) SER12 (-0.6109) SER11 (-0.575) ARG67 (0.6914 ASP65 (0.811)
	(2)		TYR155 (-0.5182)	PHE192 (-1.4785) VAL188 (-0.8822) ILE14 (-0.7667) CYS185 (-0.1326)	ASN90 (-0.391) THR190 (-0.3092) SER142 (-0.0944
	(3)	GLY92 (-0.6666)	ASN90 (-0.7463) ARG37 (-0.5923)	PHE192 (-1.767) ILE14 (-0.7278) ALA91 (-0.6234)	SER12 (-0.5629) SER11 (-0.3727) VAL188 (-0.3664) CYS185 (-0.2054)

Conclusion

1- All the investigated compounds are good corrosion inhibitors for Q235 steel in 2 M HCl solution. The effectiveness of these inhibitors depends on their structures. The variation in inhibitive efficiency depends on the type and the nature of the substituent present in the inhibitor molecule.

3- The adsorption of the inhibitors are adsorbed on Q235 steel surface obeys the Temkin adsorption isotherm model

4- Double layer capacitances decrease with respect to blank solution when the inhibitor added. This fact may explained by adsorption of the inhibitor molecule on the Q235 steel surface.

5- EFM can be used as a rapid and nondestructive technique for corrosion measurements without prior knowledge of Tafel slopes
6- The results obtained from chemical and electrochemical measurements were in good agreement. The order of % IE of these investigated compounds is in the following order: compound (1) > compound (2) > compound (3).
7- Quantum chemistry calculation results showed that the heteroatoms of N and O are the active sites of the 4-aminoantipyrine compounds. It can adsorb on Fe surface firmly by donating electrons to Fe atoms and accepting electrons from 3d orbital of Fe atoms.
8- 4-Aminoantipyrine Schiff base derivatives (1-3) are efficient inhibitors of 3hb5–OXID ORDUCTASE breast cancer have been discussed.

References

1. Wahdan M.H., Hermas A.A., Morad M.S., *Mater. Chem. Phys.* 76 (2002) 111-118.
2. Bentiss F., Lebrini M., Vezin H., Lagrenee M., *Mater. Chem. Phys.* 87 (2004) 18-23.
3. Liu X., Okafor P.C., Zheng Y.G., *Corros. Sci.* 51 (2009) 744-751.
4. Al Maofari A., Ezznaydy G., Idouli Y., Guedira F., Zaydoun S., Labjar N. and El Hajjaji S., *J. Mater. Environ. Sci. 5 (2014) 2081- 2085.*
5. Barouni K., Kassale A., Albourine A., Jbara O., Hammouti B., Bazzi L., *J. Mater. Environ. Sci. 5 (2014) 456-463.*
6. Fouda A.S., Shalabi K., Elmogazy H., *J. Mater. Environ. Sci.* 5 (2014) 1691-1702.
7. Ostovari A., Hoseinieh S.M., Peikari M., Shadizadeh S.R., Hashemi S.J., *Corros. Sci.* 51 (2009) 1935-1949.
8. Bahrami M.J., Hosseinia S.M.A., Pilvar P., *Corros. Sci.* 52 (2010) 2793-2803.
9. Solomon M.M., Umoren S.A., Udosoro I.I., Udoh A.P., *Corros. Sci.* 52 (2010) 1317-1325.
10. Wang H.L., Liu R.B., Xin J., *Corros. Sci.* 46(2004) 2455-2466.
11. Solmaz R., Kardas G., Yazici B., Erbil M., *Prot. Met.* 41 (2005) 581-585.
12. Emregul K.C., Kurtaran R., Atakol O., *Corros. Sci.* 45 (2003) 2803-2817.
13. Chebabe D., Chikh Z.A., Hajjaji N., Srhiri A., Zucchi F., *Corros. Sci.* 45 (2003) 309-320.
14. Liu F.G., Du M., Zhang J., Qiu M., *Corros. Sci.* 51 (2009) 102-109.
15. Musa A.Y., Kadhum A.A.H., Mohamad A.B., Takriff M.S., *Corros. Sci.* 52 (2010) 3331-3340.
16. Khaled K.F., Amin M.A., *Corros. Sci.* 51 (2009) 1964-1975.
17. Quraishi M.A., Rafiquee M.Z.A., Khan S., Saxena N., *J. Appl. Electrochem.* 37 (2007) 1153-1162.
18. Zhang X.Y., Wang F.P., He Y.F., Du Y., *Corros. Sci.* 43 (2001)1417-1431.
19. Knag M., Bilkova K., Gulbrandsen E., Carlsen P., Sjoblöm J., *Corros. Sci.* 48 (2006) 2592-2613.
20. Wang L., Yin G.J., Yin J.G., *Corros. Sci.* 43 (2001) 1197-1202.
21. Okafor P.C., Liu X., Zheng Y.G., *Corros. Sci.* 51 (2009) 761-768.
22. Zhang J., Liu J.X., Yu W.Z., Yan Y.G., You L., Liu L.F., *Corros. Sci.* 52 (2010) 2059-2065.
23. Fouda A.S., Shalabi K., Ezzat R., *J. Mater. Environ. Sci. 6 (2015) 1022-1039.*
24. Kassou O., Galai M., Ballakhmima R. A., Dkhireche N., Rochdi A., Ebn Touhami M., Touir R., Zarrouk A., *J. Mater. Environ. Sci. 6 (2015) 1147-1155.*
25. Khalil N., *Electrochim.Acta* 48 (2003) 2635-2640.
26. Bikadi Z., Hazai E., *J. Chem. Inf.* 11 (2009) 1-15.
27. Halgren T. A., *J. Computat. Chem.* 17 (1998) 490-519.
28. Morris G.M., Goodsell D.S., *J. Comput. Chem.* 19 (1998) 1639-1662.
29. El-Sonbati A.Z., Diab M.A., El-Bindary A.A., Abou-Dobara M.I., Seyam H.A., *Spectrochim. Acta A* 104 (2013) 213-221.
30. Wiercinska A.N., Dalmata G., *Electrochim. Acta* 51 (2006) 6179-6185.
31. Yurt A., Balaban A., Kandemir S.U., Bereket G., Erk B., *Mater. Chem. Phys.* 85 (2004) 420- 426.
32. Etre A.Y., *Appl. Surf. Sci.* 252 (2006) 8521-8525.
33. Lorenz W.J., Mansfeld F., *Corros. Sci.* 21 (1981) 647-672.
34. Putilova I.N., Balezin S.A., Barannik V.P., "Metallic Corrosion Inhibitors Pergamon" Press NewYork, 1960.
35. Al-Neami K.K., Mohamed A.K., Kenawy I.M., Fouda A.S., *Monatsh. Chem.* 126 (1995) 369- 376.

36. Noor E.A., *Int. J. Electrochem. Sci.* 2(2007)996-1017.
37. Marsh J., Advanced Organic Chemistry 3rd ed Wiley Eastern New Delhi (1988).
38. Martinez S., Stern I., *Appl.Surf.Sci.* 199 (2002) 83-89.
39. Al-Khaldi M. A., Al-qahtani K. Y. J. Mater. Environ. Sci. 4 (5) (2013) 593-600.
40. Schltze J.W., Wippermann K., *Electrochim. Acta* 32 (1987) 823-831.
41. Silverman D.C., Carrico J.E., *Corrosion* 44 (1988) 280- 287.
42. Macdonald D.D., Mckubre M.C.H., "Impedance measurements in electrochemical systems" Modern Aspects of Electrochemistry, Bockris J.O'M., Conway B.E., White R.E., Eds., Plenum Press, New York 14 1982 pp. 61–150.
43. Mansfeld F., *Corrosion* 36 (1981) 301-307.
44. Gabrielli C., "Identification of Electrochemical processes by Frequency Response Analysis" Solarton Instrumentation Group, 1980.
45. El Achouri M., Kertit S., Gouttaya H.M., Nciri B., Bensouda Y., Perez L., Infante M.R., Elkacemi K., *Prog. Org. Coat.* 43 (2001) 267-273.
46. Anejjar A., Zarrouk A., Salghi R., Zarrok H., Ben Hmamou D., Hammouti B., Elmahi B., Al-Deyab S.S., *J. Mater. Environ. Sci.* 4 (2013) 583-592.
47. Mertens S.F., Xhoffer C., Decooman B.C., Temmerman E., *Corrosion* 53 (1997) 381-388.
48. Trabanelli G., Montecelli C., Grassi V., Frignani A., *J. Cem. Concr. Res.* 35 (2005) 1804-1813.
49. Trowsdate A.J., Noble B., Haris S.J., Gibbins I.S.R., Thomson G.E., Wood G.C., *Corros. Sci.* 38 (1996) 177-191.
50. Reis F.m., de Melo H.G., Costa I., *J. Electrochem. Acta* 51 (2006) 1780-1788.
51. Lagrenée M., Mernari B., Bouanis M., Traisnel M., Bentiss F., *Corros. Sci.* 44 (2002) 573-588.
52. McCafferty E., Hackerman N., *J. Electrochem. Soc.*119 (1972) 999-1009.
53. Ma H., Chen S., Niu L., Zhao S., Li S., Li D., *J. Appl. Electrochem.* 32 (2002) 65-72.
54. Kuş E., Mansfeld F., *Corros. Sci.* 48 (2006) 965-979.
55. Caigman G. A., Metcalf S. K., Holt E. M., *J. Chem. Cryst.* 30 (2000) 415-422.
56. Samie F., Tidblad J., Kucera V., Leygraf C., *Atmospheric Environ.* 39 (2005) 7362-7373.
57. Samie F., Tidblad J., Kucera V., Leygraf C., *Atmospheric Environ.* 40 (2006) 3631-3639.
58. Lukovits I., Palfi K., Bako I., Kalman E., *Corrosion* 53 (1997) 915-919.
59. Zhao P., Liang Q., Li Y., *Appl. Surf. Sci.* 252 (2005) 1596-1607.
60. Benson J.R., Jatoi I., *Future Oncol.* 8 (2012) 697- 702.
61. Beteringhe A., Racuciu C., Balan C., Stoican E., Patron L., *Adv. Mater. Res.* 787 (2013) 236-240.

(2015) ; http://www.jmaterenvironsci.com